MANGALORE UNIVERSITY

Final Synopsis

of the PhD Thesis to be submitted for the award of degree of
Doctor of Philosophy in

Computer Science

TITLE OF THE WORK

e-IRIS : Efficient algorithms for Iris Representation and Identification System

By
Sharada S Bhat,
Research Scholar

Under the Guidance of
Dr. B.H. Shekar,
Professor

Department of Post-Graduate Studies and Research in Computer Science,
Mangalore University,
Mangalagangotri-574 199

December 2019

Contents

1 Introduction **1**
1.1 Iris Biometrics 2

2 Iris Localisation and Segmentation **3**
2.1 Proposed Segmentation Strategy 4
2.2 Edge Detection 5

3 Feature Extraction and Encoding **6**
3.1 Riesz Transforms 6
3.2 Steerable Riesz Signals 7
3.3 Taylor Series Expansion (TSE) 7
3.4 Iris Representation 8

4 Multi-patches approach **9**
4.1 Approach based on Statistical Properties 10
4.2 Fragile Bits Approach 11

5 Iris code matching **12**
5.1 Weighted Mean Hamming Distance(WMHD) 12

6 Experimental Analysis **13**
6.1 Iris Databases 13
6.2 Evaluation of Iris Recognition Systems 14
6.3 Analysis of Proposed Algorithms 15
6.4 Bit level Feature Fusion 17
6.5 Dual-Eye Approach 17
6.6 Rank-t identification 18
6.7 Comparison with Existing Methods 19

7 Contribution of this research work **19**

8 Conclusion **21**

e-IRIS: Efficient algorithms for Iris Representation and Identification System

1 Introduction

Biometrics is an automated personal recognition system based on human physiological or behavioural characteristics. Rather than recognising the persons using ID card or password, biometrics relies on the biological measures like face, iris, gait, voice, hand geometry, palm print, finger print, blood vessel patterns in the retina etc. Identifying Spersons using the biological measures started back in victorian era to identify the prisoners and criminals [8], and now with the advent of computer vision and intelligent video technologies it is used extensively in the fields that include, commercial applications, government sectors and forensic science.

A biometric system is typically a pattern recognition system which recognises a person based on a feature vector, called biometric signature, obtained from a specific biological trait possessed by that person [21]. Selected biological character must be universal (all persons must possess the character), unique (different for different persons), time/age invariant (should not change over the period of time during the life time of a person) and quantifiable (should be measurable).

Based on the application context and the mode of operating, biometric recognition systems can be categorised into two types namely, authentication (verification) systems and identification systems. Both the systems have an enrollment phase, registering users biometric signature into system database. Aim of authentication systems is to validate a persons identity. For example, a person claims that she is XYZ. Her biometric signature is captured and matched with the biometric signatures of XYZ that are pre-stored in the system's database. Based on the matching result, claim is either accepted or rejected. In this case, search is against a comparatively smaller portion of the database whereas, in identification systems, search is against the entire database. Aim of identification systems is to identify a person as who she is. If match is found person is identified and if the person is not enrolled in the system's database then match is not found and the person is unidentified.

There are two major error types a biometric system would possibly generate. One is accepting the biometric signatures of two different persons (*nonmate pairs*) as of same person. It is called *false match* or *false acceptance*. Second one is rejecting the biometric signatures of the same person (*mate pairs*) as of different persons. It is referred to as *false rejection* or *false nonmatch*. A biometric system is expected to produce both the error rates very close to zero.

1.1 Iris Biometrics

Human iris is a thin circular diaphragm lying between the cornea and the lens. It is a coloured ring of tissue around the pupil through which light enters into interior of the eye. Two muscles, dilator and sphincter muscles, control the size of iris to adjust the amount of light entering the pupil. Sclera, a white region of connective tissue and blood vessels, surrounds iris. A clear covering called cornea covers iris and pupil. Pupil region generally appears darker than the iris. Iris typically has a rich pattern of furrows, ridges, and pigment spots. Spatial patterns of minute details of iris texture are determined randomly during fetal development of the eye and are different between eyes of two different persons, between the twins and even between the left and right eye of the same person [5]. An example, showing different parts of typical human eye, is displayed in Figure 1.

Iris biometrics is regarded as one of the most promising biometric technologies with high uniqueness, stability, accuracy and non-invasiveness. In case of palm print and finger print biological measures need to come into contact with the sensing devices which, in most of the cases, may not be acceptable by the individuals. Iris lends itself to non invasive identification because it is an externally visible yet, internal organ. Like human face, iris is an overt body that is available for remote assessment. However, variability that is presented in iris appearance is much more higher than that present in face. Moreover, iris templates, being smaller in size, occupy lesser storage space than face templates. Thus, high distinctiveness, high permanence and low potential for circumvention make it possible to build a robust automated iris recognition system based on currently available computer vision and pattern recognition technologies [30].

Being the most popular and well established biometric technology for human authentication as well as identification, iris biometric finds its extensive usage in commercial and banking sectors. Most of the existing works give excellent results with cooperative eye images that are acquired using NIR imaging within suitable distance (between one or two feet) and under constrained environments. These systems suffice the requirements of the applications like banking, aadhaar card etc. However, defence, forensic and surveillance applications involve non-cooperative, at-a-distance eye images taken under less imaging constrained environment. For such applications it is desired to develop an iris recognition system which can give accurate results for both authentication and identification. Non-cooperative and noisy iris images may suffer from several noise sources like reflections, off angled images, defocus blur, and occlusion by eyelids, eyelashes, hair and glasses. We have developed efficient and accurate algorithms for different phases in iris recognition systems which can be incorporated for non-cooperative and unconstrained iris images.

Design and development of an automated iris recognition system are divided into five phases: 1) iris image acquisition, 2) iris localization, 3) normalization of iris image, 4) iris texture analysis and representation, and 5) iris pattern matching and classification. In this research work, we have conducted experiments on publicly available iris databases and hence, the stage of image acquisition is omitted. Remaining phases, executed in two stages, are as shown in Figure 2.

Rest of this pre-synopsis is organised as follows. Proposed iris segmentation technique and edge detection algorithm is explained in Section 2. Iris feature extraction and en-

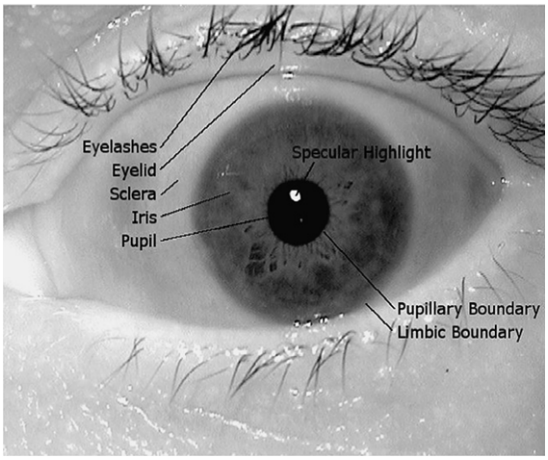

Figure 1: An example showing different parts of a typical human eye.

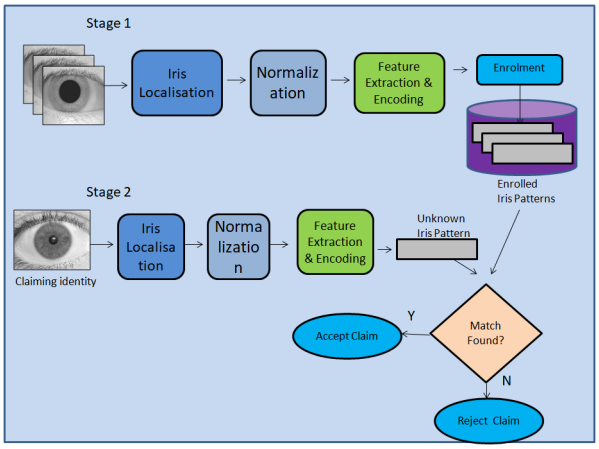

Figure 2: Two stages and different phases in an iris authentication system.

coding techniques proposed in this work are described in Section 3 and in Section 4, we have explained proposed iris recognition frame works using multi-patch approach. Iris matching is explained in Section 5. Details of the experiments, discussions on results and comparative analysis are presented in Section 6. We enumerate the publications and summarise the contributions of this work in Section 7 and Section 8 concludes this write up.

2 Iris Localisation and Segmentation

Accuracy and speed of iris recognition systems are highly dependent on efficient localization and segmentation process and hence, localization and segmentation have become crucial stages in the design of iris recognition system. Off-angled and tilted eye images made it difficult to accurately localize iris and pupil region. After locating iris boundary parameters, segmenting candidate iris region is even more complicated and time consuming task. Because, iris region would normally occluded by eye lids, eye lashes, reflections of light and spectacles.

State-of-art iris segmentation methods can be categorised into two types. First category locates pupil and iris boundaries based on edge information (boundary based methods) and second category segments candidate iris region based on pixel information (pixel-based methods) [14]. First boundary-based technique is integro-differential operator (IDO) introduced by Daugman [8], and second one is hough transform (HT) which is introduced by Wildes [30]. Various forms of IDO and HT are proposed in the literature. Apart from these methods, Shah and Ross have proposed Geodesic active counter in [26]. Pixel based methods use the information such as color, intensity variation and texture of the iris to extract discriminative appearance feature of a pixel from neighbourhood pixels [14]. Neural network classification is introduced by Proenca [22] and Sahmoud and Abuhaiba [25] have used K-means clustering and circular HT. A clustering based coarse iris localization scheme is proposed in [28] which further uses integrodifferential constellation for the localization of pupillary and limbic boundaries. Recently, Gangwar et al. [12] have proposed a boundary based course-to-fine strategy for iris localization and Liu et al. [14] have proposed iris segmentation models using convolutional neural network.

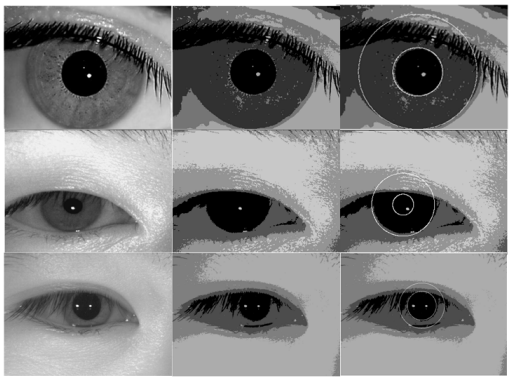

Figure 3: Column-wise: Sample images,segmented images and images with localised iris boundaries Row-wise: images from IITD, MMU v-2 and CASIA v-4 Distance databases.

Table 1: Segmentation accuracy obtained by proposed method on different databases.

Databases	Segmentation Accuracy
IIT Delhi	98.20%
MMU v-2	95.66%
CASIA v-4 Distance	90.50%

2.1 Proposed Segmentation Strategy

We have proposed a segmentation strategy which exploits both, pixel information and position with respect to other pixels in the neighbourhood, and the geometry of iris region. Iris region is segmented from the input eye image using particle swarm optimization (PSO) and then the pupil and limbic boundary parameters are located using circular Hough transform (CHT). PSO is a bioinspired theory which is first introduced by Kennedy and Eberhart [11] and has been applied to image segmentation problem by several researchers. In biometrics domain, Parez et al. have used PSO to generate templates for face and iris localization [19] and Chen and Chu have combined probabilistic neural network and PSO to design an optimized classifier model for iris recognition [7]. Inspired by these researches, we have used PSO for segmentation as PSO utilizes localized pixel information as well as global features of iris.

Output of PSO is a segmented, yet a gray scale image. We have used Canny edge detector to obtain the edge image and finally CHT is used to roughly locate the iris and pupillary boundary parameters. Located iris region may be occluded by noise such as eyelid, eye lashes, specular reflections and eye glasses. Moreover the region may not be exact circular in shape which includes some of sclera portions in the candidate iris region. Figure 3 displays sample eye images from different datasets, PSO segmented images and with extracted pupillary and iris boundaries, showing occlusion by eye lids and eyelashes.

In our experiments we have used segmentation level as 4.0 in computation of PSO segmented image. Canny edge detector (with threshold level = 2) is used to get binary edge map from PSO segmented image. Edge map thus obtained is subjected to Hough transform to coarsely locate the centers and radii of pupil and iris. While computing the segmentation accuracy we have manually noted down the correctly segmented irises and segmentation accuracy is computed as the ratio of the number of correctly segmented irises to the total number of eye images taken for the experiment. Percentages of segmentation accuracy obtained on IITD, MMU v-2 and CASIA v-4 Distance databases are given in Table 1. Our primitive interest in segmentation stage is to roughly locate iris and pupilary boundaries. Occlusion removal is achieved using multi-patches approach which is explained in Section 4

2.2 Edge Detection

Edge detection is an indispensable pace in many computer vision applications. It is one of the preprocessing steps that drastically reduces complexity of the problem and also amount of data to be processed and at the same time, retains useful boundary information. Applications like, biometrics and medical image analysis entail robust and competent edge detectors because their performance accuracy is primarily based on the efficiency of edge detectors. Though, usage of an edge detector's response is different in different applications, their expectations from an edge detector are same. Hence, there is a need of common edge detection algorithm which can be applied to different domains [6]. Generally, in an image, visually significant edges possess varieties of characteristics including texture, color and brightness and hence, finding a cohesive edge detection algorithm is difficult [10].

We propose an edge detector which is based on partial sum of second order Taylor series expansion (TSE). Infinite Taylor series expansion is a better estimator of a regular function. A regular function is a real or complex valued function which is continuously infinitely derivable. Gray scale image $f(x, y)$ is a real valued function of two variables and its directional derivative is defined as the difference in pixel values along the direction so that it can be continuously derivable and hence, TSE can be applied on gray scale image. Taylor expansion will be exact when the series is of infinite order, but if, the function is Gaussian then it is sufficient to consider a relatively small neighbourhood and compute partial sum only with finite number of terms [18]. Exploiting these properties of TSE we have applied Gaussian smoothing first and then taken a partial sum of finite terms. Representing partial sum of N terms of Taylor series expansion at θ_j^{th} orientation as $S_{\theta_j,N}$, we construct an edge operator as follows.

$$\sum_{j=1}^{M} \omega_j S_{\theta_j,N} \tag{1}$$

where, θ_j, $j \in \{1, 2, \cdots, M\}$, are M orientations and ω_j are linear coefficients. θ_j varies from 0 to 180 degrees. Using this edge operator we construct edge map $E(x, y)$ of input gray scale image $I(x, y)$ as follows:

$$E(x, y) = \left(\sum_{j=1}^{M} \omega_j S_{\theta_j,N} \right) I(x, y) \tag{2}$$

To compare the performance of proposed edge detector on gray scale images we have conducted intensive experiments on bench mark Berkeley Segmentation Dataset BSDS500 [15] Experimental results (given in terms of *F-measure*) are displayed in Table 2 and a sample iris image from IITD dataset, its segmentation result, edge map using TSE and pupilliry and iris boundaries are given in Figure 4.

Iris Normalisation: When iris and pupillary boundary parameters are obtained we can locate the candidate iris region which is having annular ring like structure. For further processing, this iris ring is transformed from Cartesian space to dimensionless polar space, in the form of a rectangular iris template, using Daugman's rubber sheet technique [8]. This process is referred to as *iris normalisation* or *unwrapping* and the rectangular iris template is referred to as *unwrapped* iris.

Table 2: Performance of edge detectors given in terms of *F-measures*.

Edge detectors	*F-measure*
TSE	0.70
Canny	0.68
Sobel	0.67
Prewitt	0.66
Roberts	0.66
LOG	0.65
ZeroCross	0.60

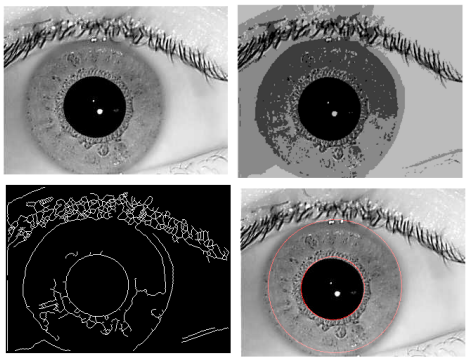

Figure 4: sample iris image from IITD dataset, its segmentation result, edge map using TSE and pupilliry and iris boundaries.

3 Feature Extraction and Encoding

Segmented iris image involves rich patterns of localized texture components like furrows, ridges and pigment spots. It possesses varied localised features. To extract unique features at local and global levels, many filters have been suggested in the literature such as Log-Gabor, Harr Wavelet, Laplacian of Gaussian, wavelet filter banks, Fourier and discrete cosine transformation (DCT), variants of LBP etc. However, to extract localised texture variations at different orientations without affecting their nativity, we have proposed following feature extraction algorithms to estimate iris function within a narrow region of iris texture.

3.1 Riesz Transforms

Our primary goal in this work is to develop an accurate and robust strategy for feature extraction and encoding of non cooperative noisy iris images. We adopt Riesz filter to extract the significant features because of its capability of capturing localized texture variations and simplicity in modeling. First order Riesz Filters can capture 1D intrinsic signals such as lines and edges in an image and second order Riesz filters can identify 2D signals like corners and junctions. Zhang et al. [31] have proposed a competitive coding technique based on Riesz Transformation for finger knuckle print verification and in [9] Depeursinge et al. have used steerable wavelets for rotation invariant texture learning.

Riesz transformations are the extensions of Hermite functions into d dimensional Euclidean space [27]. Riesz transformation R of a d dimensional function $f(x) \in L_2(R^d)$ is a vector signal which transforms a signal from $L_2(R^d)$ to $L_2^d(R^d)$, where $x = (x_1, x_2, ..., x_d)$, and is given by

$$Rf(x) = ((h_1 * f)(x), (h_2 * f)(x), ..., (h_d * f)(x)) \tag{3}$$

2D Riesz kernels are given by the following equations.

$$h_x = \frac{1}{2\pi} \frac{x}{\|x\|^3} \ , \quad h_y = \frac{1}{2\pi} \frac{y}{\|x\|^3} \tag{4}$$

$N + 1$ components of N^{th} order Riesz transform are defined as

$$R^N f = (R^{(0,N)} f, ..., R^{(n,N-n)} f, ..., R^{(N,0)} f) \tag{5}$$

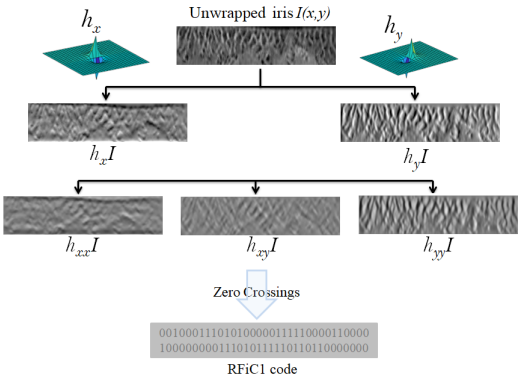

Figure 5: RFiC1 encoding process.

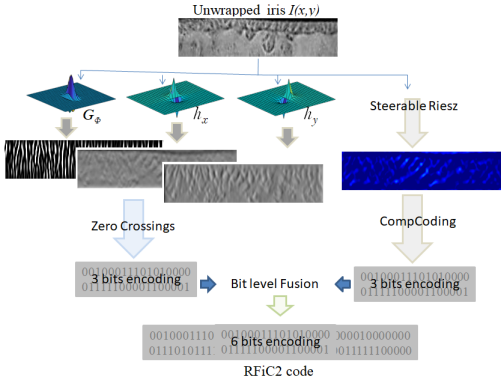

Figure 6: RFiC2 Representation.

When input signal $f(x, y)$ is convolved with the kernels given in equation (4) it produces first order monogenic Riesz signals $h_x f$ and $h_y f$. Components of second order monogenic signals $h_{xx} f$, $h_{xy} f$ and $h_{yy} f$ are obtained by convolving Riesz kernels with first order Riesz components $h_x f$ and $h_y f$.

3.2 Steerable Riesz Signals

To achieve rotation covariant features, 2D Riesz signals $h_{xx} f$, $h_{xy} f$ and $h_{yy} f$ are convolved with a steering matrix M^θ. We have adopted a 3x3 matrix as suggested by [9] and linear combination of Riesz wavelet components is obtained by following equation:

$$Rf^\theta(x, y) = \omega_1 M^\theta h_{xx} f(x, y) + \omega_2 M^\theta h_{xy} f(x, y) + \omega_3 M^\theta h_{yy} f(x, y) \tag{6}$$

where ω_1, ω_2 and ω_3 are the weights assigned to Riesz components. At every pixel (x, y) in input image f an integer Q which varies from 0 to $m - 1$, where m is the number of orientations, is computed as follows,

$$Q(\theta) = argmax_\theta(Rf^\theta(x, y)) \tag{7}$$

θ takes m orientations, $\frac{k\pi}{m}$, $k = 0, 1, ..., m - 1$. In our experiments we have taken $m = 6$, generating a matrix consisting of integers from one to six, specifying dominant orientation. Input iris image is then coded into binary iris code by representing dominant orientation with corresponding binary bits, $\{000, 001, 011, 111, 110, 100\}$.

3.3 Taylor Series Expansion (TSE)

Further, we have proposed another feature extraction technique that uses partial sum of first N terms of second order Taylor series expansion (TSE), N being a finite number, which can work on different scales. Partial sum of TSE, computed with finite number of terms can very well represent the local iris features with less errors. We have computed partial sum on multiple scales to capture finest variations of iris texture. In [4], authors have used only second and third coefficients of TSE which are based on first and second order derivatives computed separately at eight different scales and have encoded them based on zero crossings of convolution outputs.

To compute higher order derivatives involved in the Taylor's sum we have devised derivative kernels using binomial coefficients and extending the Sobel kernel. For illustration, extended kernels to compute third and fourth order derivatives $\frac{\partial^3}{\partial\theta^3}I(r,\theta)$ and $\frac{\partial^4}{\partial\theta^4}I(r,\theta)$ of the iris $I(r,\theta)$, along horizontal direction are given below. Here $I(r,\theta)$ is unwrapped iris template in $r\theta$ space.

$$\begin{bmatrix} -1 & -3 & -3 & -1 \\ 0 & 0 & 0 & 0 \\ 0 & 0 & 0 & 0 \\ 1 & 3 & 3 & 1 \end{bmatrix} \qquad \begin{bmatrix} -1 & -4 & -6 & -4 & 1 \\ 0 & 0 & 0 & 0 & 0 \\ 0 & 0 & 0 & 0 & 0 \\ 0 & 0 & 0 & 0 & 0 \\ 1 & 4 & 6 & 4 & 1 \end{bmatrix}$$

Normalised iris is convolved with the above kernels to obtain corresponding derivatives and we have calculated two partial sums for each pixel, namely radial sum and angular sum using following equations.

$$AngularSum = \sum_{n=1}^{N}(\theta-\eta)^n\frac{1}{n!}\frac{\partial^n}{\partial\theta^n}I(\xi,\eta) \tag{8}$$

$$RadialSum = \sum_{n=1}^{N}(r-\xi)^n\frac{1}{n!}\frac{\partial^n}{\partial r^n}I(\xi,\eta) \tag{9}$$

Angular sum is obtained by taking partial derivatives along $\theta - axis$ and Radial sum is obtained by partial derivatives along $r - axis$ at a point $(r,\theta) = (\xi,\eta)$. Scale factors $\varepsilon = \theta - \eta$ and $\delta = r - \xi$ are the small quantities along θ and r axes and are determined, based on the resolutions of θ and r taken for normalisation. If m and n are number of resolutions of θ and r respectively and then values of ε and δ can be computed using the following equations.

$$\varepsilon_i = \frac{1}{m}(\theta_{max} - \theta_{min}) * i, \quad \delta_j = \frac{1}{n}(r_{iris} - r_{pupil}) * j \tag{10}$$

where θ_{min} and θ_{max} are the minimum and maximum values through which θ varies during normalisation and r_{iris} and r_{pupil} are the radii of iris and pupil regions respectively. By changing these scale factors along respective directions, partial sums can be computed at different scales.

3.4 Iris Representation

We have developed four iris representation algorithms. RFiC1, RFiC2 and RSBP are Based on Riesz responses and using Taylor series outputs TSE encoding algorithm is designed.

RFiC1: The Riesz kernels, h_x and h_y, given in Equation (3.1) are operated on input unwrapped iris, $I(x,y)$ to obtain first order responses h_xI and h_yI and then, these outputs are again operated by the kernels to obtain second order responses, $h_{xx}I$, $h_{xy}I$ and $h_{yy}I$. We get totally five Riesz kernel responses, giving amplitude and phase information at each pixel which are encoded in to 5 binary bits using 1D phase encoding technique. Pictorial representation of RFiC1 which describes an input pixel with 5 binary bits is explained in Figure 6.

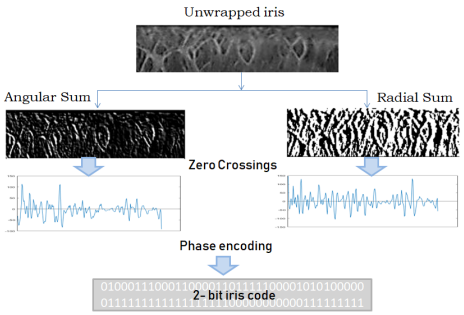

Figure 7: 2-bit TSE representation.

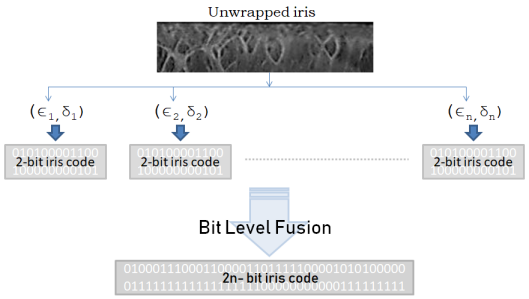

Figure 8: n-bit representation of TSE.

RFiC2: Our second algorithm maps input unwrapped iris into a binary code wherein, each pixel is described by 6 bits. Here first three bits are zero crossings output of the triplet $\langle G_\theta f, h_x f, h_y f \rangle$ where $G_\theta f$ is Gabor filter response at the orientation θ and $h_x f$, $h_y f$ are the responses of 1D Riesz signals. Remaining three bits are obtained by steerable Riesz wavelet method explained in Section 3.2. This method is demonstrated pictorially in Figure **??**.

TSE Descriptor: In case of TSE filter (Section 3.3), at each input pixel, radial and angular sums are obtained using equations (8) and (9) and then the pixel is encoded by binary bits based on zero crossings of the responses of these sums. In case of multi-scale TSE, radial and angular sums are computed at n different scales and bits generated by output at each scale are concatinated to obtain a $2n$ bit representation for each pixel. Figure **??** explains working of TSE approach at single scale and and in Figure **??** we have presented multi-scale TSE approach.

RSBP Descriptor: RSBP is designed using monogenic components of first and second order Riez and steerable wavelets. Responses of each of these first and second order monogenic components are encoded into a binary bit, 0 or 1, using 1D phase informations of zero crossings, so that, each input pixel (x, y) is represented by five binary bits. Further, steerable Riesz produces three more binary bits based on the dominant orientation. combining these bits we obtain a binary pattern of 8-bits for every input pixel. We convert this 8-bit binary digits into corresponding decimal number. While computing the decimal equivalent of this binary pattern, we have taken response of first order Riesz along horizontal direction as the most significant bit (MSB) and last bit in steerable Riesz output as least significant bit (LSB). RSBP image patch is subdivided into P number of $p_1 \times q_1$ sized *sub-blocks*. In every sub-block, we compute k bin length histogram. Further, histograms of all of these sub blocks are concatenated to obtain 1D feature vector. RSBP algorithm is explained in Figure 9.

4 Multi-patches approach

The technique of region-wise, multi-patch feature extraction is previously used by the researchers at classification stage [23, 4, 20]. In most of the unconstrained eye images upper and lower region are usually occluded by eyelids. Some authors ([4]) ignore the sectors which contains upper and lower iris portion and do not involve them in the feature extraction process. We have not completely omitted these regions. Because, occluded

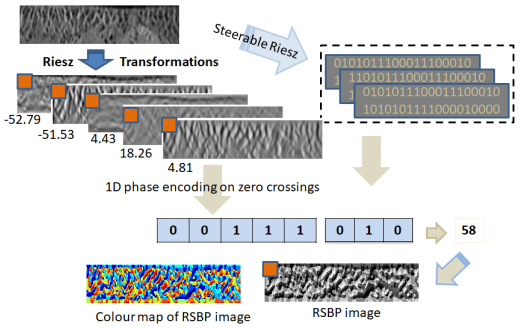

Figure 9: RSBP approach.

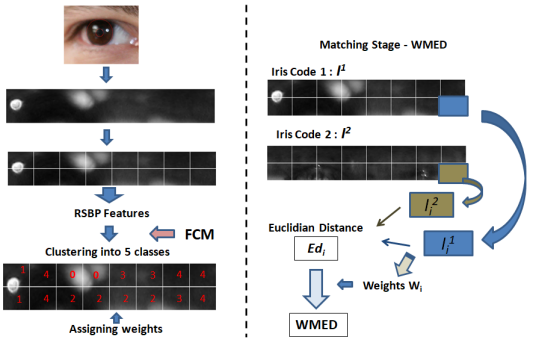

Figure 10: Multi-patches approach using RSBP.

portion is not uniform across all eye images of the same subject. It varies from image to image. We have used circular Hough transform to roughly identify pupil and iris boundary parameters. At this stage, actual parameters are not identified. Because, segmented iris is not in exact circular shape. Moreover, candidate iris region is encompassed with noise and occlusion such as, eyelids, eyelashes and photographic reflections. Some surrounding non-iris portion and some un-useful part of pupil may also be present. This will reduce percentage of accuracy drastically. In Figure 3, segmented iris and roughly identified circular structure of candidate iris region are shown for some sample eye images taken from three benchmark datasets. It can be seen that candidate iris region is occluded by eyelids, eyelashes and some adjacent non-iris portion. Not all the portion of segmented iris is useful for recognition task.

In order to obtain the portion of candidate iris region which can be used for further processing we have adopted multi-patches technique. Annular iris ring is divided into N patches using m tracks and n sectors. Daugman's doubly dimensionless rubber sheet model [8] is used to unwrap the iris into uniform sized iris templates. Figure 11 shows an analytical model of annular ring which is divided into 16 patches using two sectors and eight tracks. Further, these patches are classified into five classes with labels best-iris, iris, moderate, less-moderate and no-iris and accordingly weights from 0 to 4 are assigned to them. In order to classify the iris patches we have developed two methods. First one utilises the statistical properties using probability density function of each patch and second method uses fragile bit count. Later fuzzy c-means clustering (FCM) is adopted to cluster them into five clusters.

4.1 Approach based on Statistical Properties

The probability density function of each patch is separately computed. Based on these properties, patches of iris are grouped into clusters using Fuzzy c-means clustering. The motivation behind using Fuzzy clustering is that the Fuzzy matching is used by [29] to match the two different irises. Properties of iris patches are fuzzy in nature and they possess close statistical relationships. FCM is a well suited tool for such data. We have observed the cluster output and the ground truth of iris and have trained the system to assign the weights to the patches.

During the experiments we have selected first 20 eye images from each database. The segmented iris is divided into 16 patches using 2 tracks and 8 sectors. These 16 patches are

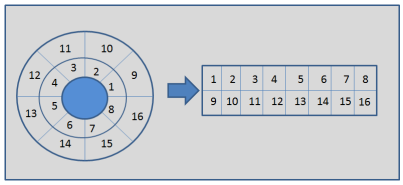

Figure 11: Analytical model of annular iris ring divided into 16 patches using 2 tracks and 8 sectors, and its unwrapped template.

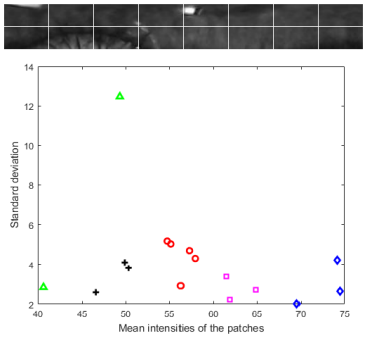

Figure 12: An example of iris patches and graphical representation of the clustered output given by FCM.

clustered into 5 groups. We have computed the probability density function of each patch and a 2D vector of mean and standard deviation is given as input to FCM. The cluster output and the manually computed ground truth of the 16 patches are compared and accordingly weights are assigned to them as $1, 0.75, 0.5, 0.25, 0.0$ representing, best iris, iris, partially iris, less partially iris and no iris respectively. An example of iris patches and graphical representation of the clustered output is shown in Figure 12.

4.2 Fragile Bits Approach

In case of unconstrained imaging, statistical properties cannot accurately cluster noisy regions because there exists multiple noise resources and noisy regions possess both dark and light pixels. Moreover, while unwrapping the annular ring of iris, pupillary and iris boundaries are taken as circular rings but, in most of the images, actual iris region is not in exact circular shape. This adds some regions of sclera to unwrapped iris. In order to handle such problems we propose fragile bits approach.

Fragility refers to the inconsistency of an iris bit in attaining the value 0 or 1 across iris codes of irises of the same subject. Let $\mathcal{P}(x)$ be the probability that a bit x flips between 0 and 1 among all images of the same subject. If a bit x is captured accurately without occlusion and without any capturing errors, then $\mathcal{P}(x) \to 0$ and it is called a consistent bit. Otherwise it is a fragile bit.

A practical approach to fragile bit is proposed in [13]. Let $\mathcal{N}$ be the total number of irises of a subject taken for experimentations. If a bit attains 1's for more than a τ percent of $\mathcal{N}$ irises it is considered as consistent bit and if a bit attains 0's for more than τ percent of times, it is taken as consistent as well. Thus, in order to identify fragile bits we propose following definition.

Definition 4.1. Let $\mathcal{O}(x_n)$ and $\mathcal{Z}(x_n)$ be number of 1's and 0's attained by a bit x_n, respectively, across $\mathcal{N}$ irises. For an arbitrary bit x define a function $\mathcal{F}(x)$ as,

$$\mathcal{F}(x) = \frac{|\mathcal{O}(x) - \mathcal{Z}(x)|}{\mathcal{N}} \tag{11}$$

Then, x_n is said to be fragile if,

$$\lim_{x \to x_n} \mathcal{F}(x) = \lim_{x \to x_n} \frac{|\mathcal{O}(x) - \mathcal{Z}(x)|}{\mathcal{N}} = 0 \tag{12}$$

When it is operated on real irises, function $\mathcal{F}(x)$ becomes a discrete function. Hence, above definition may be simplified as; a bit x_n is fragile if $\mathcal{F}(x_n) < \epsilon$ where ϵ is a sufficiently small positive quantity.

In this approach we adopt RSBP descriptor to learn fragile bits in each patch. FCM is trained with manually classified patches based on RSBP feature vector. RSBP can very well capture the predominant features which are rich enough to identify pixels that generate fragile bits. Similar to first approach iris patches are ranked based on FCM output. This frame work is explained in Figure 10.

5 Iris code matching

Final task in iris recognition system is to match and classify the iris codes to agree upon a particular decision to accept or reject a particular claim or to identify a person. To match two iris codes either a similarity score or dissimilarity score is computed. Majority of the researchers use technique proposed by Daugman, in order to find the dissimilarity score between the two iris codes. This approach uses Hamming distance which basically uses XOR operation. We have applied Hamming distance to find the dissimilarity between two iris codes in case of non-multi-patches approach. Whereas, in case of multi-patches approach we have used weighted mean Hamming distance which is explained in the following Section.

5.1 Weighted Mean Hamming Distance(WMHD)

Let $\mathcal{I}^1$ and $\mathcal{I}^2$ be two iris codes to be matched. $\mathcal{I}_i^1$ and $\mathcal{I}_i^2$ be i^{th} patches of these codes and ω_i^1 and ω_i^2 be the weights assigned to these patches where $i \in \{1, 2, ...N\}$, N being the total number of patches. Let d_i be the dissimilarity score between the patches $\mathcal{I}_i^1$ and $\mathcal{I}_i^2$, computed using Hamming distance. We have applied arithmetic and geometric means and maximum value strategies on ω_i^1 and ω_i^2 in order to compute common weight. Taking ω_i as common weight for both $\mathcal{I}_i^1$ and $\mathcal{I}_i^2$, weighted mean distance is calculated by,

$$d(\mathcal{I}^1, \mathcal{I}^2) = \frac{\sum \omega_i d_i}{\sum \omega_i} \tag{13}$$

When both $\mathcal{I}_i^1$ and $\mathcal{I}_i^2$ have non zero weights, ω_i will be the maximum of the weights ω_i^1 and ω_i^2 and when both have zero weights then ω_i will have zero weight. However, if one of them say, $\mathcal{I}_i^1$ has zero weight and $\mathcal{I}_i^2$ has high weight then, fragile bits of $\mathcal{I}_i^1$ when compared with bits of $\mathcal{I}_i^2$ would decrease the matching accuracy and hence, in third case we set zero value for ω_i. Thus,

$$\omega_i = \begin{cases} 0, & if \;\; \omega_i^1 = 0 \;\; or \;\; \omega_i^2 = 0 \\ max\left(\omega_i^1, \omega_i^2\right), & otherwise \end{cases} \tag{14}$$

In Figure 13, we have illustrated computational procedure of weighted mean Hamming distance. In second approach, which uses RSBP featues, we adopt weighted mean Euclidean distance (WMED) because the iris codes we obtain here are 1D real valued feature vectors (This frame work is explained in Figure 10.

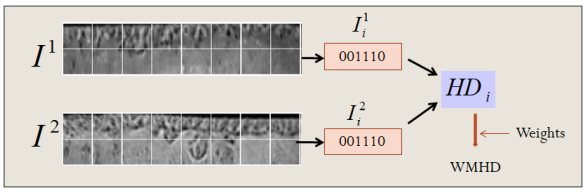

Figure 13: Illustration of computation procedure of weighted mean Hamming distance (WMHD).

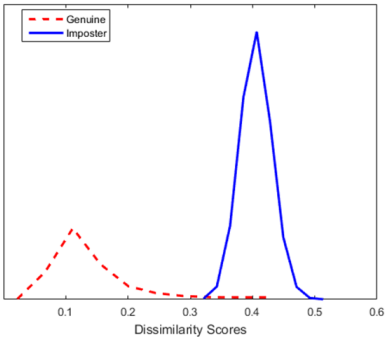

Figure 14: Genuine and imposter distributions obtained using proposed TSE method with respect to IITD database.

6 Experimental Analysis

In this Section, we discuss the merits of our proposed techniques, compare them with other techniques and discuss the demerits if there exists any. In order to justify the suitability of proposed algorithms, we have conducted rigorous experiments on four different datasets IITD, MMUv-2, CASIS v4 Distance and UBIRIS v-2 and we have compared the results with the results obtained using existing methods such as, discrete cosine transform (DCT) [17] and Log-Gabor [16]. Eye images collected from any database are preprocessed before using them for actual treatments of recognition process. Preprocessing step involves, smoothing, using low pass Gaussian filter, histogram equalization and gamma corrections. In following Sections, we brief the databases used for experimentation.

6.1 Iris Databases

We have used publicly available benchmark databases including near infra red (NIR) images and images with visible wavelength (VW images). All databases have degraded images which we could use to train and test our algorithms. Sample images from different datasets are shown in Figure 15. Usage of these NIR and VW images for constructing training and test data subsets is explained in the experiment analysis given in the next sections.

IITD Database: IIT Delhi database [1] consists of 2240 eyes of 224 users between the age group 14 to 55 years comprising of 176 males and 48 females, collected by NIR imaging. This database has degraded noisy eyes with occlusions by eye lids and eye lashes, containing 10 eyes of each subject where first five are left eyes and next five are right eyes. This database has degraded noisy eyes with occlusions by eye lids and eye lashes captured in the indoor environment.

MMU v-2 Database: MMU v-2 [3] has varieties of off angled, non cooperative and occluded eyes of 99 subjects with 10 eye images for each subject and similar to IITD database, first five are left eye images and next five are right eye images. Images are acquired in both indoor and outdoor environments using NIR imaging.

CASIA v-4 Distance Database: CASIA v4 Distance is a subset of CASIA v4 [2] database which consists of wide varieties of non cooperative and noisy eye images captured through NIR imaging at a distance of three meters. This database has 2567 eye images of 142 subjects with a minimum of 10 images of each subject. Each image has dual-eye iris from which patterns of left and right irises can be independently accessed.

UBIRIS v.2 Database: UBIRIS version 2.0 [24] database comprises of 11102 iris images from 261 subjects. This database has highly corrupted, disoriented (off-angled) images taken form a distance of 4 to 8 meters which are acquired through visual wavelength (VW) imaging. Each subject has not lesser than 30 images with 15 left eye images and 15 right eye images.

Sample images from the above four databases are presented in Figure 15. One can observe occluded, off-angled and noisy eye images samples.

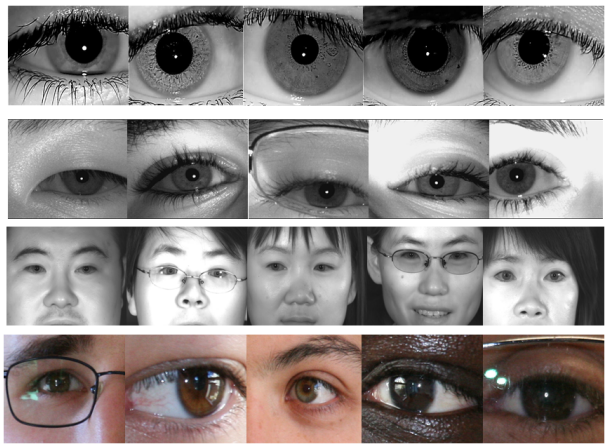

Figure 15: Row-wise: Sample images from IITD, MMU v-2, CASIA v4 Distance and UBIRIS v.2, respectively.

6.2 Evaluation of Iris Recognition Systems

In order to evaluate proposed algorithms and to compare the results with the existing techniques, we use two quantitative measures namely decidability index ($d-prime$ value) and equal error rate (EER) and a graphical method, receiver operating characteristic (ROC) curve (false acceptance rate v/s genuine acceptance rate). All these three measuring techniques are based on the two distributions, namely, distribution of *genuine scores* and *impostor scores*. In Figure 14 we have presented genuine and impostor distributions obtained using proposed TSE method with respect to IITD database.

Dissimilarity score between the two irises of the same person is called *genuine score* and between the irises of two different persons is called *imposter score*. If μ_i and σ_i are mean and standard deviation of imposter distribution and μ_g and σ_g are those of genuine distribution then $d-prime$ is given by the following formula. A higher $d-prime$ value indicates better performance.

$$d-prime = \frac{|\mu_i - \mu_g|}{\sqrt{\frac{1}{2}(\sigma_i^2 + \sigma_g^2)}} \tag{15}$$

EER is a point on ROC curve where genuine acceptance rate is equal to false reject rate. Lower EER value indicates better performance of a biometric system. In order to to compute EER and $d-prime$ values, we calculate genuine and imposter distributions for each database separately and we draw ROC curve for each database.

To evaluate identification systems, a graphical metric, cumulative match characteristic (CMC) curve which plots *rank-t* identification rates against t ranks, where $t = 1, 2, 3, ..., N$ is used.

6.3 Analysis of Proposed Algorithms

RFiC1: We have investigated a novel approach RFiC1 for feature extraction and encoding of noisy, off angled, at-a-distance iris images with high accuracy. We have also demonstrated that Riesz filter's performance is on par with Gabor filter. Higher order Riesz filters, compared to Gabor or any other like filters, are giving equally good results and most importantly, are easy to implement and possess less computational complexity with smaller window size (15 x 15 in our experiments). Another merit of RFiC1 approach is, its simplicity in implementing. Expressions given in equations 4 can be easily implemented. Results of our experiments given in Table 3 illustrate that RFiC1 approach performs better than existing methods.

One demerit of this approach is, deviations are computed along horizontal and vertical axes. Though, most of the localised feature can be extracted from these two directions, since iris features vary along all directions, it needs to tune the algorithm in this direction and hence, we tried steerable Riesz wavelets.

RFiC2: One of the objectives of our work is to develop a feature extraction and encoding scheme for iris images acquired under less constrained, at-a-distance environment. To extract robust features, local organizations of intensities in all directions of iris region are to be properly characterized. In order to recognize identical pattern instances in iris textures that have different local orientations, rotation invariant features are required. Though rotation invariant features do not vary when an image is transformed, they fail to notice the local directional information [9]. Hence, we have explored rotation covariant features which, on transformation, vary with respect to some transformation function and hence, can capture local directional variations. Steerable Riesz filters are the most suitable filters for both rotation invariant and covariant features.

Proposed RFiC2 method captures iris features in all directions and hence, performs better than RFiC1 approach. Though, size of the iris code is increased (2D Riesz encodes an iris template into five bit iris code whereas, RFiC encodes it into six bit iris code), performance of RFiC2 is better than that of RFiC1. We have presented the results ($d-prime$ and EER values) obtained using both RFiC1 and RFiC2 along with existing methods DCT and Log-Gabor with respect to three NIR databases in Table 3.

TSE Approach: Above two algorithms outperforms with the existing methods, however we wanted to design a feature extraction algorithm which is more simple and accurate. We have proposed a method which uses linear combination of derivatives of first, second and higher order terms and which, we observed, is more efficient method compared to RFiC1 and RFiC2. Further, radial and angular sums given in equations (8) and (9) are

Table 3: The d prime values and EER obtained by different methods on IITD, MMU v-2 and CASIA v-4 Distance.

Method	IITD		MMU v-2		CASIA v-4 dist	
	EER	d'	EER	d'	EER	d'
DCT[17]	0.0809	2.6703	0.1749	1.8686	0.2788	1.1710
Log-Gabor[16]	0.0246	5.4817	0.0810	2.8218	0.1132	2.3916
RFiC1(proposed)	0.0228	5.6306	0.0575	3.3081	0.0952	2.5549
RFiC2(proposed)	0.0206	5.8188	0.0636	3.3864	0.0879	2.7280

Table 4: Comparison of RFiC1, RFiC2 and TSE methods using EER and $d-prime$ values with respect to three NIR databases

Method	IITD		MMU v-2		CASIA v-4 dist	
	EER	$d-prime$	EER	$d-prime$	EER	$d-prime$
RFiC1	0.0228	5.6306	0.0575	3.3081	0.0952	2.5549
RFiC2	0.0206	5.8188	0.0636	3.3864	0.0879	2.7280
TSE	0.0279	5.8728	0.0542	3.3948	0.0871	2.7349

computed taking different scales can capture iris texture variations at different resolutions of r and θ which has increased the recognition accuracy. This fact is demonstrated by the results displayed in Table 4.

TSE approach is simple to implement. Time taken by any convolution operation involved in the feature extraction techniques depends on both, the size of input image as well as size of the kernel. Largest kernel entailed in the proposed method is of size five and hence, computational time taken by proposed method is less compared to existing methods which involve larger size kernels. To illustrate this, we have computed time taken per computation by different methods and have presented them in Table 5.

Multi-pathces Approach: To circumvent the problem of occlusion in the segmented iris, we have used the concept of multi-patches. Algorithms proposed in Section 3 are experimented using both the multi-patches approach described in Section 4. In Table 6 we

Table 5: The computation time taken by different methods.

Method	Time taken per computation (in seconds)
Gabor	1.33E-02
DCT	1.10E-02
Log-Gabor	6.42E-03
TSE	2.23E-03

give the results obtained by proposed algorithms using non-multi-patch and multi-patch approach. We can observe that multi-patches using fragile bits and RSBP (second approach) gives better results compared to multi-patches using probability density functions and FCM (first approach) with respect to IITD database. ROC curves displayed in Figure 16 demonstrates graphical representation of these results.

Table 6: Experimental results obtained using non-multi-patches approach, using multi-patches with probability density functions and FCM (approach 1) and lastly using multi-patches with fragile bits and RSBP (approach 2) on different methods with respect to IITD database.

	Without multi-patches		Multi-patches Approach 1		Multi-patches Approach 2	
Method	EER	$d-prime$	EER	$d-prime$	EER	$d-prime$
RFiC1	0.0228	5.6306	0.0220	5.6311	0.0207	5.6321
RFiC2	0.0212	5.7134	0.0217	5.7561	0.0206	5.8188
TSE	0.0279	5.8728	0.0198	5.8796	0.0200	5.8811
RSBP	0.0195	5.9910	0.0190	6.0038	**0.0173**	**6.1137**

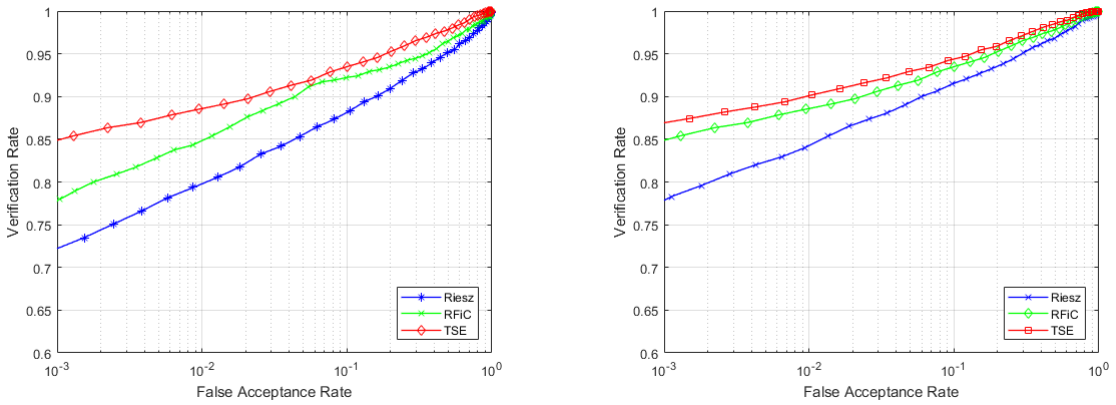

Figure 16: ROC curves obtained by proposed algorithms experimented on CASIA v-4 Distance database using without-multi-patches and with-multi-patches-fragile-bit approach.

6.4 Bit level Feature Fusion

During our work we have carried out experiments using the concept *feature fusion*. Two or more filters are used to extract iris features. Then, we have fused these filter responses at bit level. For illustration, Gabor filter generates a two bit representation and a 2D Riesz filter generates three bit representation, fusion of these two iris codes would generate five bit representation for a pixel. In Table 7 we have presented the results of different filters and their fusion. It can be observed that when the responses of two or more filters are fused tough, the size of the iris code increases, percentage of accuracy is also increased. Graphical representation of these results are displayed in Figure 17.

6.5 Dual-Eye Approach

During the experimentation we have tried a dual-eye approach. We have extracted the features from both left and right irises, encode them separately into two binary iris codes

Table 7: Recognition rates obtained by different feature extraction methods and their fusion on the three NIR databases. Training to test ratio is 3:2 taking kNN classifier.

Method	IITD	MMU v-2	CASIA v-4 dist
Gabor	92.50	85.50	80.00
Riesz	95.00	86.34	82.50
TSE	97.50	87.00	85.00
Gabor+Riesz	93.33	87.50	85.00
Gabor+TSE	97.66	90.00	85.00
Riesz+TSE	98.50	92.33	87.50
Gabor+Riesz+TSE	98.96	95.67	90.00

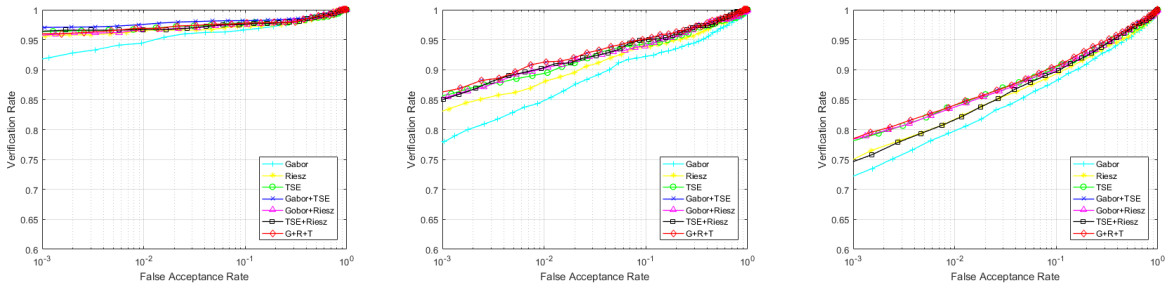

Figure 17: ROC curves obtained by different algorithms and their fusion with respect to IITD, MMU v-2 and CASIA v-4 Distance databases, respectively.

and then combine the binary codes by concatenating the bits of corresponding pixel position in both the irises to produce a combined iris code. Experimental results have proved that dual-eye approach obtained by combining the features of left and right eyes performs better than sole eye approach.

Fusion approach increases the size of the iris code. To avoid this expansion in size, we have modified the proposed methods a little. In Gabor + Riesz filter, left iris is encoded with two Gabor bits and right iris is encoded with two first order Riesz. In RFiC2, left iris is encoded with 3 bits using second order Riesz wavelets and right iris is encoded with three more bits using steerable Riesz wavelets. In RFiC1 each of left and right irises are encoded into 5 bits hence, doubling the size of iris code. Results of these experiments are shown in Table 8. These results reveal that the accuracy is increased as compared to sole eye feature extraction approach.

6.6 Rank-t identification

To substantiate the applicability of our approaches for iris identification systems, we have carried out the experiments on IITD, MMU v-2, CASIA v-4 Distance and UBIRIS v.2 datasets and Rank-t identification accuracies are computed. During these experiments we have taken training to test ratio as 3:2. In Figure 18 and 19 we have presented CMC curves with respect to CASIA v4 Distance and UBIRIS v.2 datasets obtained by proposed algorithms.

Table 8: Comparison of sole eye approach and combined approach (fusion of left and right irises) using d prime values and EER obtained by different methods on IITD.

Method	Sole eye approach		Combined approach	
	EER	d'	EER	d'
DCT	0.0809	2.6703	0.0514	3.4619
Gabor	0.0246	5.4817	0.0058	6.0770
RFiC1	0.0228	5.6306	0.0046	7.3389
RFiC2	0.0206	5.8188	0.0041	6.0884

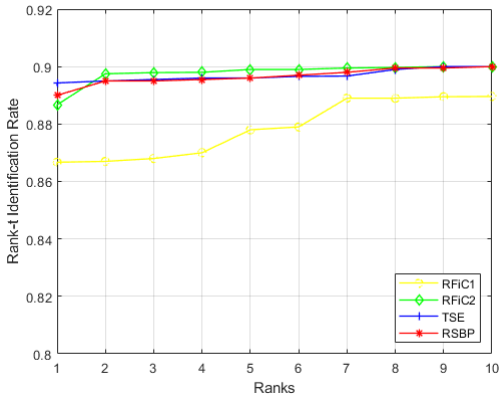

Figure 18: CMC for CASIA v-4 Distance

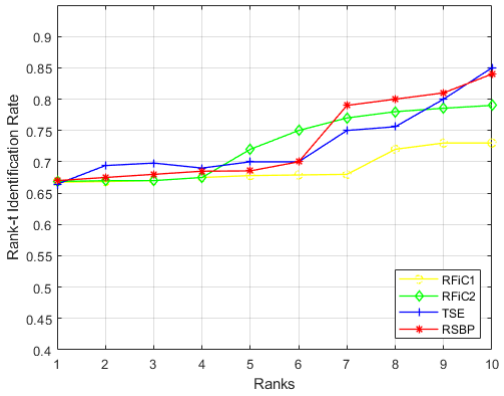

Figure 19: CMC for UBIRIS v.2.

6.7 Comparison with Existing Methods

To justify the applicability of proposed algorithms, we have carried out the experiments with publicly available state-of-the-art iris tool boxes under similar experimental set-up which has been used to evaluate proposed algorithms. Open source iris recognition systems used in comparative analysis are, Masek'implementation, IrisBEE, VeriEye SDK and OSIRIS. Recognition rates (RR) obtained by these tools and proposed algorithms are shown in Figure 20. Datasets involved in computing RR are, CASIA v1, UBIRIS v.1, MMU v-1, IIT Delhi, CASIA v-4 Distance, CASIA v-3 Interval and MMU v-2.

7 Contribution of this research work

In this section, we enlist the contributions of this work which are justified through extensive experimental analysis.

- We have explored second order Riesz wavelets to extract localised intricate iris features and have developed three iris feature extraction and encoding algorithms RFiC1, RFiC2 and RSBP based on first and second order monogenic components of Riesz and steerable wavelets.
- We have explored application of partial sum of second order Taylor series expansion for iris feature extraction. A novel and accurate feature extraction and encoding algorithm (TSE algorithm) is developed for noisy, off angled, at-a-distance iris images.

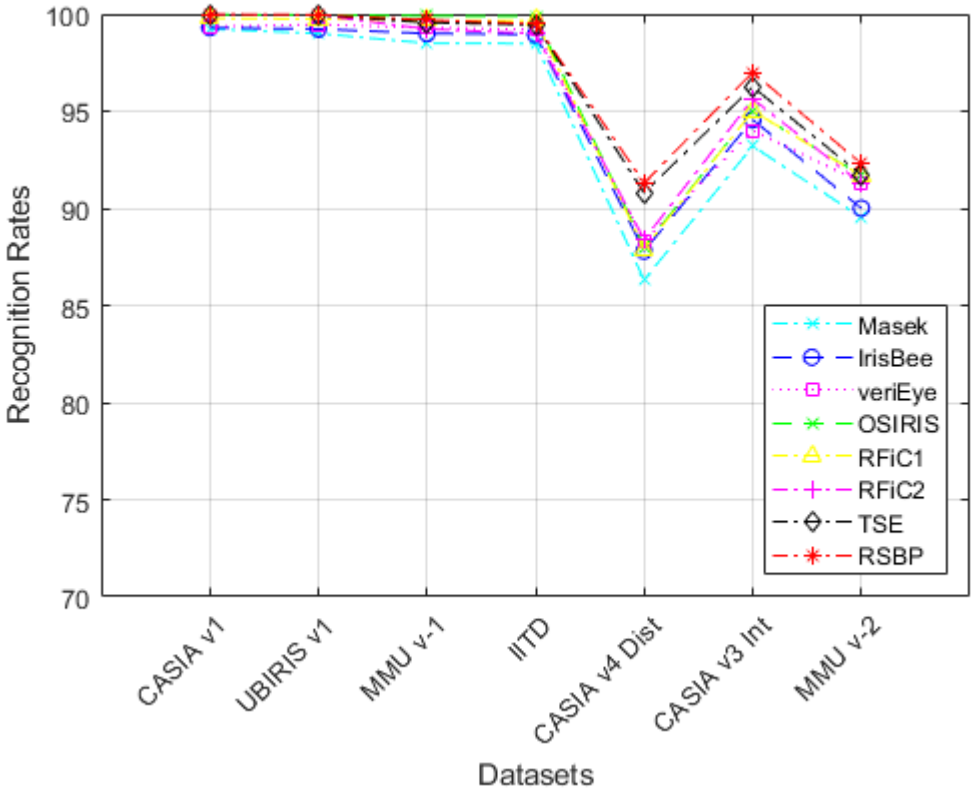

Figure 20: Recognition rates obtained by existing iris identification tools and proposed algorithms on different datasets.

- We have devised an iris segmentation and localisation method to coarsely locate the iris and pupillary boundary parameters by adopting of particle swarm optimisation (PSO) and circular Hough transform (CHT).
- A novel, simple and generic edge detector has been designed to detect the edges in a gray scale image, using partial sum of Taylor series expansion, which is a gradient based approach that outperforms with the classical gray scale edge detectors. Its applicability for iris localisation has been justified empirically.
- We have designed two iris recognition frame works using multi-patches approach and fuzzy c means clustering (FCM). First one utilises probability density function of the patches and second one uses bit fragility to rank them as best-iris to no-iris.
- In multi-patches approach, in order to match the iris codes of multi-patches with different weights, weighted mean distances have been proposed and a strategy has been devised to compute the common weight.
- Extensive experiments have been carried out by considering feature fusion at bit level and dual-eye approach. Comparative analysis of proposed algorithms has been performed with the existing methods.

8 Conclusion

We have developed efficient and robust iris feature extraction and encoding algorithms for noisy, off-angled, at-a-distance iris authentication and identification systems. A method is proposed to locate iris and pupillary boundary parameters. Two iris recognition frameworks have been designed for unconstrained imaging using multi-patches approach. In order to justify their sustainability, proposed algorithms have been tested on benchmark datasets.

Published Work

1. B H Shekar, Sharada S Bhat. Steerable Riesz wavelet based approach for iris recognition. 3rd IAPR Asian Conference on Pattern Recognition (ACPR), p: 431-436, Publisher:IEEE, 2015.

2. B H Shekar, Sharada S Bhat. Iris recognition using partial sum of second order Taylor series expansion. Proceedings of the Tenth Indian Conference on Computer Vision, Graphics and Image Processing (ICVGIP 16), p: 81, Publisher: ACM, 2016.

3. B H Shekar, Sharada S Bhat. Multi-Patches iris based Person Authentication System using Particle Swarm Optimization and Fuzzy C-Means Clustering. The International Archives of Photogrammetry, Remote Sensing and Spatial Information Sciences (ISPRS), Volume XLII-2/W4, 2nd International ISPRS Workshop on PSBB, 15–17 May 2017, Moscow, Russia2017, Volume: 42, Pages: 243, Publisher: Copernicus GmbH.

4. BH Shekar, Sharada Bhat, Archil Maysuradze. Reliability Index for Iris Code Matching in Iris Recognition Systems. ISPRS, Volume XLII-2/W12, International Workshop on *Photogrammetric & Computer Vision Techniques for Video Surveillance, Biometrics and Biomedicine*, 13–15 May 2019, Moscow, Russia.

5. B H Shekar, Sharada Bhat, Leonid Mestetsky. Iris Recognition by Learning Fragile Bits on Multi-patches using Monogenic Riesz Signals. International Conference on Pattern Recognition and Machine Intelligence PReMI 2019, Volume: 11942, Issue: Lecture Notes in Computer Science (LNCS), Pages: 462-471, Publisher: Springer, 2019.

Communicated

1. B H Shekar, Sharada Bhat. Edge Detection in Gray Scale Images using Partial Sum of Second Order Taylor Series Expansion. International Journal, IET Image Processing at IET Digital Library.

2. B H Shekar, Sharada Bhat. Iris Biometrics using Circular Harmonic Vectors based on Higher order Riesz Transforms. IET Biometrics at IET Digital Library.

3. B H Shekar, Sharada Bhat, Rathnakar Shetty. Multi-modal Biometrics for Face, Iris and Fingerprint Authentication using hand-crafted Filter banks. International Journal of Biometrics (IJBM).

References

[1] Indian Institute of Technology, Delhi, India, Iris Database. http://www4.comp.polyu.edu.hk/csajaykr/IITD/Database_Iris.htm/.

[2] Institute of Automation, Chinese Academy of Sciences. CASIA Iris Database. http://biometrics.idealtest.org/.

[3] Malaysia Multimedia University Iris Database. http://pesona.mmu.edu.

[4] Algirdas Bastys, Justas Kranauskas, and Volker Krüger. Iris recognition by fusing different representations of multi-scale taylor expansion. *Computer Vision and Image Understanding*, 115(6):804–816, 2011.

[5] Kevin W Bowyer, Karen Hollingsworth, and Patrick J Flynn. Image understanding for iris biometrics: A survey. *Computer vision and image understanding*, 110(2):281–307, 2008.

[6] John Canny. A computational approach to edge detection. *IEEE Transactions on Pattern Analysis and Machine Intelligence*, (6):679–698, 1986.

[7] Ching-Han Chen and Chia-Te Chu. High performance iris recognition based on 1-d circular feature extraction and pso–pnn classifier. *Expert Systems with Applications*, 36(7):10351–10356, 2009.

[8] John G Daugman. High confidence visual recognition of persons by a test of statistical independence. *IEEE transactions on pattern analysis and machine intelligence*, 15(11):1148–1161, 1993.

[9] Adrien Depeursinge, Antonio Foncubierta-Rodriguez, Dimitri Van de Ville, and Holger Muller. Rotation–covariant texture learning using steerable riesz wavelets. *Image Processing, IEEE Transactions on*, 23(2):898–908, 2014.

[10] Piotr Dollár and C Lawrence Zitnick. Fast edge detection using structured forests. *IEEE Transactions on Pattern Analysis and Machine Intelligence*, 37(8):1558–1570, 2015.

[11] Russ C Eberhart, James Kennedy, et al. A new optimizer using particle swarm theory. In *Proceedings of the sixth international symposium on micro machine and human science*, volume 1, pages 39–43. New York, NY, 1995.

[12] Abhishek Gangwar, Akanksha Joshi, Ashutosh Singh, Fernando Alonso-Fernandez, and Josef Bigun. Irisseg: A fast and robust iris segmentation framework for non-ideal iris images. In *Biometrics (ICB), 2016 International Conference on*, pages 1–8. IEEE, 2016.

[13] Karen P Hollingsworth, Kevin W Bowyer, and Patrick J Flynn. The best bits in an iris code. *IEEE Transactions on Pattern Analysis and Machine Intelligence*, 31(6):964–973, 2009.

[14] Nianfeng Liu, Haiqing Li, Man Zhang, Jing Liu, Zhenan Sun, and Tieniu Tan. Accurate iris segmentation in non-cooperative environments using fully convolutional networks. In *Biometrics (ICB), 2016 International Conference on*, pages 1–8. IEEE, 2016.

[15] D. Martin, C. Fowlkes, D. Tal, and J. Malik. A database of human segmented natural images and its application to evaluating segmentation algorithms and measuring ecological statistics. In *Proc. 8th Int'l Conf. Computer Vision*, volume 2, pages 416–423, July 2001.

[16] Libor Masek and Peter Kovesi. Matlab source code for a biometric identification system based on iris patterns, the university of western australia, 2003, 2013.

[17] Donald M Monro, Soumyadip Rakshit, and Dexin Zhang. Dct-based iris recognition. *Pattern Analysis and Machine Intelligence, IEEE Transactions on*, 29(4):586–595, 2007.

[18] Pedro J Moreno, Bhiksha Raj, and Richard M Stern. A vector taylor series approach for environment-independent speech recognition. In *Acoustics, Speech, and Signal Processing, 1996. ICASSP-96. Conference Proceedings., 1996 IEEE International Conference on*, volume 2, pages 733–736. IEEE, 1996.

[19] Claudio A Perez, Carlos M Aravena, Juan I Vallejos, Pablo A Estevez, and Claudio M Held. Face and iris localization using templates designed by particle swarm optimization. *Pattern recognition letters*, 31(9):857–868, 2010.

[20] Jaishanker K Pillai, Vishal M Patel, Rama Chellappa, and Nalini K Ratha. Secure and robust iris recognition using random projections and sparse representations. *IEEE Transactions on Pattern Analysis and Machine Intelligence*, 33(9):1877–1893, 2011.

[21] Salil Prabhakar, Sharath Pankanti, and Anil K Jain. Biometric recognition: Security and privacy concerns. *IEEE security & privacy*, 99(2):33–42, 2003.

[22] Hugo Proenca. Iris recognition: On the segmentation of degraded images acquired in the visible wavelength. *IEEE Transactions on Pattern Analysis and Machine Intelligence*, 32(8):1502–1516, 2010.

[23] Hugo Proenca and Luis A Alexandre. Toward noncooperative iris recognition: a classification approach using multiple signatures. *IEEE Transactions on Pattern Analysis and Machine Intelligence*, 29(4):607–612, 2007.

[24] Hugo Proenca, Silvio Filipe, Ricardo Santos, Joao Oliveira, and Luis A Alexandre. The UBIRIS.v2: A database of visible wavelength iris images captured on-the-move and at-a-distance. *IEEE Transactions on Pattern Analysis and Machine Intelligence*, 32(8):1529–1535, 2010.

[25] Shaaban A Sahmoud and Ibrahim S Abuhaiba. Efficient iris segmentation method in unconstrained environments. *Pattern Recognition*, 46(12):3174–3185, 2013.

[26] Samir Shah and Arun Ross. Iris segmentation using geodesic active contours. *IEEE Transactions on Information Forensics and Security*, 4(4):824–836, 2009.

[27] Krzysztof Stempak and José Luis Torrea. Poisson integrals and riesz transforms for hermite function expansions with weights. *Journal of functional analysis*, 202(2):443–472, 2003.

[28] Tieniu Tan, Zhaofeng He, and Zhenan Sun. Efficient and robust segmentation of noisy iris images for non-cooperative iris recognition. *Image and vision computing*, 28(2):223–230, 2010.

[29] Chung-Chih Tsai, Heng-Yi Lin, Jinshiuh Taur, and Chin-Wang Tao. Iris recognition using possibilistic fuzzy matching on local features. *IEEE Transactions on Systems, Man, and Cybernetics, Part B (Cybernetics)*, 42(1):150–162, 2012.

[30] Richard P Wildes. Iris recognition: an emerging biometric technology. *Proceedings of the IEEE*, 85(9):1348–1363, 1997.

[31] Lin Zhang and Hongyu Li. Encoding local image patterns using riesz transforms: With applications to palmprint and finger-knuckle-print recognition. *Image and Vision Computing*, 30(12):1043–1051, 2012.

Research Candidate:

Sharada S Bhat,
Research Scholar,
Department of Computer Science,
Mangalore University

Research Supervisor:

Dr. B.H. Shekar,
Professor,
Department of Computer Science,
Mangalore University